ADVANCED FUNCTIONAL MATERIALS

FULL PAPER

DOI: 10.1002/adfm.200800056

The Relation Between Open-Circuit Voltage and the Onset of Photocurrent Generation by Charge-Transfer Absorption in Polymer : Fullerene Bulk Heterojunction Solar Cells**

By *Koen Vandewal,** *Abay Gadisa, Wibren D. Oosterbaan, Sabine Bertho, Fateme Banishoeib, Ineke Van Severen, Laurence Lutsen, Thomas J. Cleij, Dirk Vanderzande,* and *Jean V. Manca*

Photocurrent generation by charge-transfer (CT) absorption is detected in a range of conjugated polymer–[6,6]-phenyl C_{61} butyric acid methyl ester (PCBM) based solar cells. The low intensity CT absorption bands are observed using a highly sensitive measurement of the external quantum efficiency (*EQE*) spectrum by means of Fourier-transform photocurrent spectroscopy (FTPS). The presence of these CT bands implies the formation of weak ground-state charge-transfer complexes in the studied polymer–fullerene blends. The effective band gap (E_g) of the material blends used in these photovoltaic devices is determined from the energetic onset of the photocurrent generated by CT absorption. It is shown that for all devices, under various preparation conditions, the open-circuit voltage (V_{oc}) scales linearly with E_g. The redshift of the CT band upon thermal annealing of regioregular poly(3-hexylthiophene):PCBM and thermal aging of poly(phenylenevinylene)(PPV):PCBM photovoltaic devices correlates with the observed drop in open-circuit voltage of high-temperature treated versus untreated devices. Increasing the weight fraction of PCBM also results in a redshift of E_g, proportional with the observed changes in V_{oc} for different PPV:PCBM ratios. As E_g corresponds with the effective bandgap of the material blends, a measurement of the *EQE* spectrum by FTPS allows us to measure this energy directly on photovoltaic devices, and makes it a valuable technique in the study of organic bulk heterojunction solar cells.

1. Introduction

Currently, the best performing polymer-based solar cells comprise bulk heterojunction (BHJ) polymer/acceptor interpenetrating networks characterized by a three dimensional, nanoscale morphology. The generation of photocurrent in such solar cells follows a multi-step process, namely, generation of excited electron-hole pairs (excitons), mainly in the polymer phase and the subsequent splitting of these excited states at the polymer/acceptor interface leaving free holes in the polymer phase while transferring the electrons to the electron accepting material. Such a transfer process eventually leads to two separate percolation paths for the free charge carriers.[1,2] Successful BHJ devices have been fabricated by solution deposition of mixtures of a soluble conjugated polymer and the fullerene derivative [6,6]-phenyl C_{61} butyric acid methyl ester (PCBM). Among the commonly used soluble conjugated polymers are poly(phenylene vinylene) (PPV),[3,4] polyfluorene[5,6] and polythiophene[7] derivatives. By controlling the BHJ nanomorphology, power conversion efficiencies up to 4–5% have been achieved.[7,8] However, further improvements are still needed in order to obtain higher efficiencies that make polymer solar cells competitive with their inorganic counterparts.

Understanding the factors that limit photovoltaic parameters such as short-circuit current (J_{sc}) and open-circuit voltage (V_{oc}), helps to optimize material and device structures, leading to higher efficiencies. While J_{sc} is determined by the creation and subsequent dissociation of excitons at the polymer/acceptor interface followed by transport of free charge carriers towards the collecting electrodes[9], V_{oc} is primarily determined by the effective band gap of the BHJ film.[10,11]

As far as the exciton dissociation process is concerned, recent theories and experimental evidences indicate that an intermediate charge-transfer (CT) state exists between the excitons created upon light absorption in the polymer and the long-lived, free charge carriers. Recently, the existence of such an intermediate CT state in a BHJ consisting of a low band gap semiconducting copolymer and PCBM was inferred from analysis of its carrier recombination dynamics.[12] Quantum chemical calculations of charge transfer in the

[*] K. Vandewal, Dr. W. D. Oosterbaan, S. Bertho, Dr. F. Banishoeib, Dr. I. Van Severen, Dr. L. Lutsen, Prof. T. J. Cleij, Prof. D. Vanderzande Prof. J. V. Manca
Institute for Materials Research, Hasselt University
Wetenschapspark 1, 3590 Diepenbeek (Belgium)
E-mail: koen.vandewal@uhasselt.be
Dr. A. Gadisa, Dr. L. Lutsen, Prof. D. Vanderzande, Prof. J. Manca
IMEC-IMOMEC, vzw
Wetenschapspark 1, 3590 Diepenbeek (Belgium)

[**] This research was funded by the IWT-projects Nanosolar and Polyspec, the interreg project OLED+ and the FWO projects G.0396.08 and G.0091.07. K. V. acknowledges the institute for the promotion of innovation through science and technology in Flanders (IWT-Vlaanderen) for funding. S. B. is a research assistant of the Fund for Scientific Research Flanders (FWO-Vlaanderen).

ADVANCED FUNCTIONAL MATERIALS

poly(3-hexylthiophene) (P3HT):PCBM material system also support the presence of an extended electronic state created upon material blending.[13] It was shown that this state has a significant probability distribution across the donor/acceptor (D/A) interface in its lowest excited state. The existence of such intermediate bound electron-hole pairs at the D/A interface was already assumed to explain the compositional dependence of the photocurrent generation in PPV:PCBM solar cells.[14] It was shown that the incomplete dissociation of these photo-generated bound electron-hole pairs under operating conditions is a main loss mechanism in this type of solar cells. Further optimization of polymer–fullerene based solar cells thus requires a thorough study of these interfacial intermediate states.

Highly sensitive studies of the absorption spectra of P3HT:PCBM and PPV:PCBM blends by our group, have revealed the presence of a long wavelength absorption band characteristic for a weak ground state CT complex (CTC), formed by the interaction of the lowest unoccupied molecular orbital of the fullerene acceptor LUMO(A) with the highest occupied molecular orbital of the polymer donor HOMO(D).[15–16] Illumination with wavelengths in this CT band results in the direct creation of bound electron-hole pairs or CT excitons, as described by Foster[17] for CTCs in solution.

CTC formation is widely observed when combining donor materials with electron acceptors such as C_{60} and C_{70} (see for example reference[18] and references therein). Recently, it was shown that a whole range of π-conjugated polymers and oligomers form CT absorption bands when mixed with electron acceptors in chloroform solution.[19] Using Photothermal Deflection Spectroscopy and photoluminescence spectroscopy, the formation of CTCs was also evidenced for solid-state blends of different types of polyfluorenes with PCBM.[20–21]

In reference[21] a model for the involvement of these CTCs in the photocurrent generation mechanism was proposed. It was shown that the energy of the excited CTC is critical for determining whether photocurrent is generated, or energy transfer and subsequent emission from the PCBM singlet state takes place. In previous works involving CTCs, however, no correlation between the open-circuit voltage and this CTC state has been reported.

In order to do so, we have measured the external quantum efficiency (*EQE*) spectra of photovoltaic devices consisting of a variety of conjugated polymers blended with PCBM by means of Fourier-transform photocurrents spectroscopy (FTPS). Originally applied to investigate subgap absorption by defects in hydrogenated microcrystalline silicon for photovoltaic devices, FTPS has a superior sensitivity[22] as compared to monochromatic photocurrent measurement techniques. When applied to organic BHJ devices, it can be used for the determination of the device's absorption window. Moreover, FTPS has the required sensitivity to measure the low signal sub-band gap photocurrent produced by the direct creation of CT excitons upon long wavelength illumination of the CTCs.[16]

In this paper it will be shown that the effective bandgap (E_g), determined by the onset of photocurrent generation by CT absorption, linearly correlates with the V_{oc} of the studied devices. Regardless of device type and treatment conditions such as annealing and aging a difference between the $\frac{E_g}{e}$ and V_{oc} of about 0.43 V was observed for measurements performed at room temperature and under 1 sun illumination conditions. This investigation provides a deeper understanding of the origin of the photovoltage of polymer:PCBM based solar cells and hence may help to engineer material structures that lead to improved performance of BHJ solar cells.

2. Results and Discussion

2.1. Photocurrent Generation by CT Absorption

We have characterized various organic BHJ solar cells by measuring the *EQE* as a function of photon energy (*E*), using FTPS. The *EQE* is defined as the number of photo-generated electrons flowing in the external circuit at short-circuit, per incident photon.

A typical *EQE* spectrum of a polymer BHJ solar cell (active layer of MDMO-PPV:PCBM in a 1:4 weight ratio, sandwiched

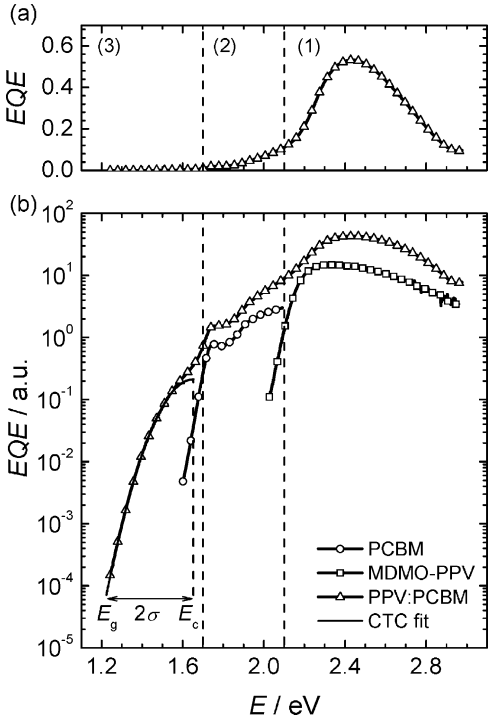

Figure 1. The external quantum efficiency (*EQE*) as a function of the energy (*E*) of the incident light of the MDMO-PPV:PCBM (1:4) photovoltaic device measured by FTPS presented on a) a linear and b) a logarithmic scale. The different spectral regions (1)–(3) are described in the text. In figure (b) the FTPS spectra of the pure materials are also represented (in arbitrary units). The non-additive CTC band can be fitted with a Gaussian function centred at E_c and with a standard deviation σ. We define the effective band gap E_g as $E_g = E_c - 2\sigma$, as shown in the figure.

between ITO/PEDOT:PSS and Ca/Al electrodes) is shown in Figure 1 on a linear (a) and on a logarithmic (b) scale.

In Figure 1(b), the photocurrent spectra of the pure materials sandwiched between ITO/PEDOT:PSS and Al are also shown (on an arbitrary scale) for comparison. The *EQE* spectrum depicted in Figure 1(b) shows typical features that have different origins. The rightmost region (1), with photon energies greater than 2.1 eV, corresponds to the absorption spectrum of MDMO-PPV. The photocurrent generated in this region thus mainly originates from the excited states created in the polymer. Moreover, for the MDMO-PPV:PCBM blend, high values of *EQE* are achieved in this region indicating that polymer absorption is the primary source of excitons. The *EQE* in the second region (2), located between 1.7 eV and 2.1 eV, mainly represents the absorption of the acceptor molecule PCBM. The distinct peak around 1.75 eV is due to the symmetry forbidden optical HOMO-LUMO transition in the PCBM phase.[15] The spectrum in the leftmost region (3), with photon energies between 1.2 eV and 1.7 eV, does not overlap with the absorption spectrum of either pure MDMO-PPV or PCBM. Based on the justifications given in previous reports,[15,16,21] we attribute this low energy band to the CTCs created at the interface of MDMO-PPV and PCBM.

The new band occuring in the *EQE* spectrum originates from the absorption of long wavelenght photons by the CTC ground states, giving rise to a direct creation of charge-separated states. The bound electron-hole pairs created by this CT absorption are separated further, generating photocurrent. Very recently[23] it was argued that photocurrent generation occurs more efficiently through a 'hot' CT state, than through a relaxed state. This would make the CT exciton splitting efficiency wavelength dependent. Efforts are currently underway to investigate the energetic dependence of the splitting efficiency of the CT excitons.

As the ground state interaction in a polymer:PCBM CTC is expected to be weak, the spectral position of the CT band correlates to the difference of the polymer's HOMO level and the PCBM's LUMO level.[17,19] For MDMO-PPV this difference has been determined from cyclic voltammetry measurements to be around 1.4 eV (Table 1). This value is well below the bandgap of both MDMO-PPV (2.1 eV) and PCBM (1.7 eV), and is in the observed spectral range of the CT band (1.2–1.6 eV) in the *EQE* spectrum.

The absorption coefficient of the CT absorption in MDMO-PPV:PCBM blends, as determined by PDS, is well below 1000 cm^{-1}.[15] This makes the *EQE* spectral shape of the CT band independent of device thickness (thicknesses of our devices are typically around 100 nm). We have also found that the spectral shape of the CT band is not affected by electrode material, and is very reproducible for devices having the same polymer:PCBM weight ratio. Furthermore, the spectral shape of the CT band can be well fitted with a Gaussian function with amplitude A_0, centered around E_c and given by the equation $A(E) = A_0 \exp[-(E - E_c)^2/(2\sigma^2)]$. Henceforth, we define the onset E_g of the photocurrent generation by CT absorption as:

$$E_g = E_c - 2\sigma \quad (1)$$

The difference between the onset and the maximum of the CT band, $E_g - E_c$, is related to the reorganization energy between the Franck-Condon excited state D^+-A^- and the relaxed D^+-A^- excited state geometry.[24,25] In addition, the presence of CTC conformers with slightly different geometries and hence different energies of the CT state might also contribute to the width of the CT band. The CTC band gap E_g, which is much lower than the lowest band gap of the materials in the D/A blend, can be considered as the effective bandgap E_g of the BHJ films. The Gaussian fit and the involved parameters are indicated in Figure 1. By using this description of the CT band, the correlation of the energy of the lowest CT state capable of generating photocurrent, with the photovoltaic parameters of the solar cells is discussed in the next section of this paper.

The mechanism of charge dissociation, involving the CTC has previously been discussed.[21,23] The excitons generated either in the polymer or in the PCBM phase (region (1) and (2) in Figure 1) diffuse to the interface, where the intermediate CT exciton (an excited CTC) is formed. At this stage, the CT exciton is still coulombically bound and may either decay to the CTC ground-state or be converted into a more loosely bound polaron-pair state. Upon illumination in the spectral region (3) of Figure 1, however, CT excitons are directly created. As the CTC has a much lower absorption coefficient as compared to the polymer, the contribution of the photocurrent generated by this direct CT absorption is marginal as compared to the overall photocurrent of the BHJ photovoltaic device.

Table 1. Solar cell characteristic parameters for several polymer:PCBM BHJ devices and their LUMO(A)–HOMO(D) gaps as determined by cyclic voltammetry.

Donor Polymer	D/A ratio	J_{sc} [mA.cm^{-2}]	V_{oc} [V]	*FF*	$E_{LUMO(A)}$ - $E_{HOMO(D)}$ [eV]	E_c [eV]	E_g [eV]
MDMO-PPV	1:4	3.9	0.83	0.53	1.4	1.65	1.22
OC9-PEO-PPV	1:4	2.1	0.65	0.50	1.2	1.68	1.14
RR-P3HT	1:1	7.9	0.62	0.56	1.3	1.80	1.08
Dihexyl-PTV	1:1	1.7	0.57	0.49	1.2	1.42	1.02

ADVANCED FUNCTIONAL MATERIALS

2.2. Influence of the HOMO Level of the Donor Polymer on E_g and V_{oc}

We have measured the photovoltaic properties of several types of solar cells with varying polymer:PCBM BHJ active films. The chemical structures of the investigated conjugated polymers are depicted in Figure 2.

We have determined the important parameters of the photovoltaic devices such as J_{sc}, V_{oc} and fill factor (*FF*) by measuring current-voltage characteristics under 100 mW/cm^2 AM1.5 solar illumination. The E_g of the corresponding blends was determined from their *EQE* spectra measured by FTPS, as described in the previous section. The FTPS spectra, obtained in the spectral region between 1.0 and 2.0 eV, of the photovoltaic devices consisting of different donor polymers (diHexyl-PTV, PEO-OC9-PPV, MDMO-PPV and P3HT) in their best performing polymer:PCBM ratios are depicted in Figure 3. All four polymers show CTC formation upon mixing with PCBM. CTC formation was confirmed by the presence of a low energy, Guassian like, CT band for all devices. The presence of this sub-bandgap feature is expected in this region since the energy differences between the LUMO level of PCBM and the HOMO levels of the donor polymers (Table 1) are positioned far below the onsets of the absorption bands of the pure materials. For visibility, the fitted CT spectum of each device is normalized.

The relation between V_{oc} and E_g is shown in the inset of Figure 3, and it is shown that V_{oc} indeed scales with E_g of the D/A material blend. J_{sc} and *FF*, however, do not show a clear trend as can be seen from Table 1. The latter parameters in fact depend strongly on charge transport, absorption coefficient and morphology of the active layer.

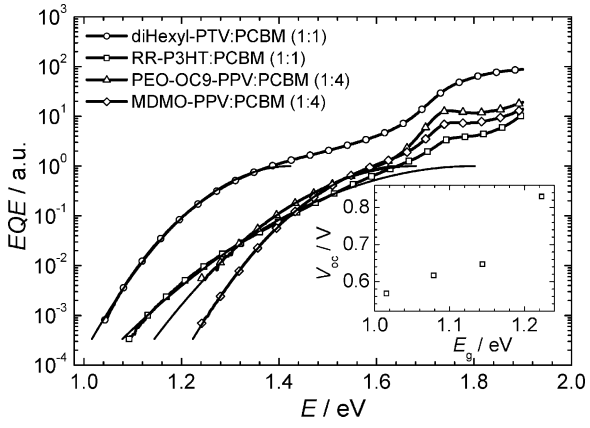

Figure 3. FTPS spectra of different types donor polymers blended with PCBM in the spectral area 1.0 eV $< E <$ 2.0 eV. The CT absorption band was fitted with a Gaussian and the band gap was determined as described in the text. The inset shows the open-circuit voltage V_{oc} versus the effective band gap E_g.

2.3. Influence of Morphology on E_g and V_{oc}

It is well documented that the V_{oc} of P3HT:PCBM based solar cells reduces slightly upon annealing. Such changes have been attributed to morphological changes.[26,27] Figure 4 shows the FTPS spectra of three types of solar cells: 1) regiorandom (ReRa) P3HT as electron donor, 2) non-annealed and regioregular (RR) P3HT as electron donor, 3) annealed and regioregular P3HT as electron donor.

The electron acceptor is PCBM in all cases, mixed with the polymers in a 1:1 weight ratio. In the case of RR-P3HT, it is known that an annealing procedure improves the crystallisation of the polymer phase, which improves the mobility of the charge carriers and causes a redshift in the absorption spectrum.[27] This crystallinity enhancement results in a clear improvement of both *FF* and J_{sc}. In the case of ReRa-P3HT:PCBM, the morphology does not show any crystallinity at all, and therefore the solar cells exhibit a low *FF* and J_{sc}. These results are summarised in Table 2. From this table and Figure 4 it is clear that the improved crystallinity causes a redshift of the onset of the CT band, resulting in a proportional reduction of V_{oc}.

To investigate the effect of morphological aging on the CTC energy in more detail, photovoltaic devices were fabricated using MDMO-PPV or "High T_g-PPV" as electron donor material, blended in a 1:4 weight ratio with PCBM. Upon thermal aging at 110 °C, PCBM clusters are relatively rapidly formed in

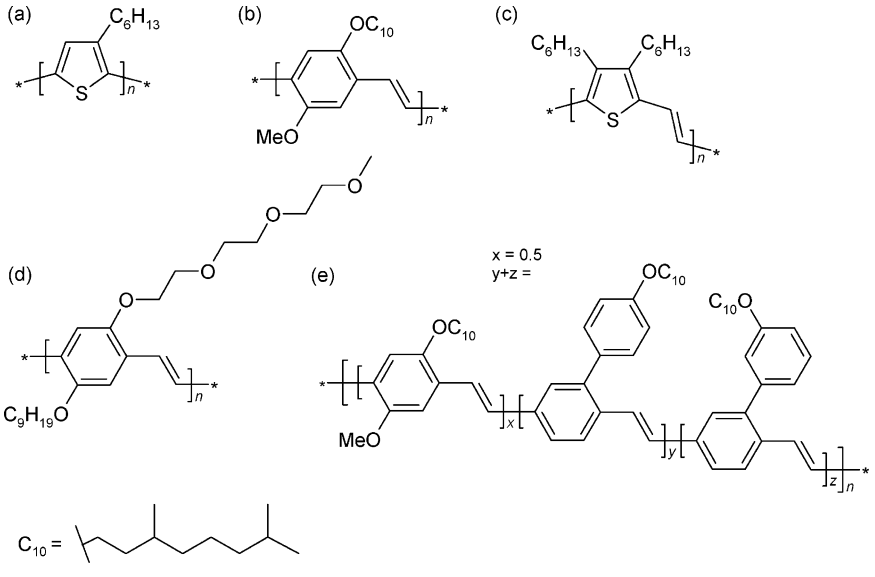

Figure 2. The chemical structure of a) P3HT, b) MDMO-PPV, c) diHexyl-PTV, d) PEO-OC9-PPV, and e) "High T_g-PPV". In this work the regiorandom and regioregular form of P3HT are used.

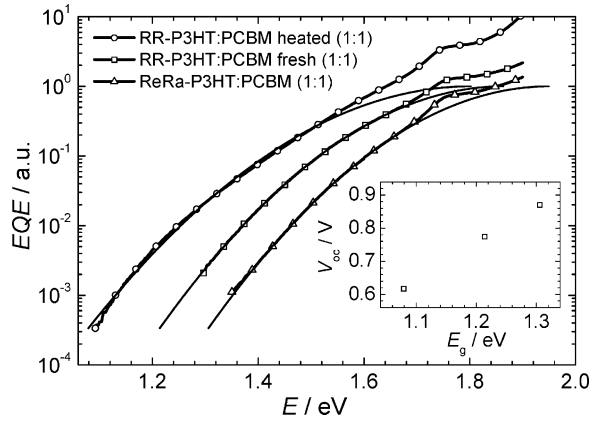

Figure 4. FTPS spectra of different types of P3HT blended with PCBM in the spectral area $1.0 < E < 2.0$ eV. The CT absorption band was fitted with a Gaussian and the effective band gap was determined as described in the text. The inset shows the open-circuit voltage V_{oc} versus the effective band gap E_g.

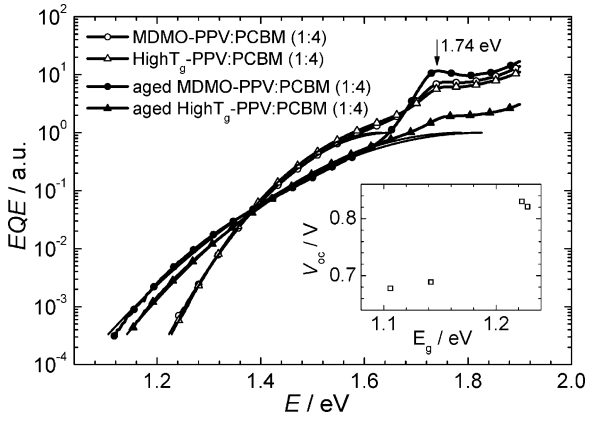

Figure 5. FTPS spectra of fresh and thermally aged MDMO-PPV:PCBM and "High T_g-PPV":PCBM photovoltaic devices in the spectral area of $1.0 < E < 2.0$ eV. The CT absorption band was fitted with a Gaussian and the band gap was determined as described in the text. The inset shows the open-circuit voltage V_{oc} versus the effective band gap E_g.

the MDMO-PPV:PCBM devices, while the morphology of the "High T_g-PPV":PCBM devices stays rather unchanged. This is due to the higher glass transition temperature T_g of "High T_g-PPV" ($T_g \approx 138\,^{\circ}C$) as compared to that of MDMO-PPV ($T_g \approx 12\,^{\circ}C$).[28] Photovoltaic parameters for freshly prepared and for thermally aged (16 h at 110 °C) devices are given in Table 3.

From this table it is clear that J_{sc} is severely reduced by thermal aging for solar cells based on MDMO-PPV as compared to those based on "High T_g-PPV". In contrast, the V_{oc} and the onset energy of the CT band (Figure 5) degraded equally in both devices.

The formation of a more course phase separated morphology in thermally aged MDMO-PPV:PCBM blends [28] can be identified in the FTPS spectra: for the aged MDMO-PPV–PCBM device, the PCBM photocurrent peak at 1.74 eV becomes more pronounced due to the formation of PCBM aggregates. Upon aging, the amount of CTCs thus decreases, indicating less D/A material interaction, and thus a more phase separated morphology. In the case of "High T_g-PPV", the amount of complexes stays relatively unchanged upon thermal aging, indicating a more stable morphology[28] as expected from its higher T_g.

In the case of RR-P3HT the observed redshift is explained by an increase in the polymer's HOMO level upon crystallisation. For the PPVs, it is known that a large scale crystallisation does not take place upon annealing. However, the formation of aggregates upon annealing of PPVs, resulting in an increased amount of polymer interchain interaction, has been observed.[29] On the other hand, phase separation is only detected in the case of MDMO-PPV.[28] We conclude that similarly as in the case of RR-P3HT:PCBM, the formation of aggregates created upon thermal aging of both types of PPV:PCBM based devices increases the effective HOMO level of the polymer and leads to the shift in CT energy and the corresponding drop in V_{oc}.

Table 2. Solar cell characteristic parameters for photovoltaic bulk heterojunction devices consisting of P3HT with a different degree of crystallinity.

Donor Polymer	Heat treatment	J_{sc} [mA.cm^{-2}]	V_{oc} [V]	*FF*	E_c [eV]	E_g [eV]
ReRa-P3HT	no	0.73	0.87	0.29	1.95	1.31
RR-P3HT	no	3.5	0.77	0.36	1.86	1.21
RR-P3HT	yes	7.9	0.62	0.56	1.80	1.08

Table 3. Solar cell characteristic parameters for fresh and thermally aged photovoltaic bulk heterojunction devices consisting of MDMO-PPV and "High-T_g-PPV".

Donor Polymer	Aged	J_{sc} [mA.cm^{-2}]	V_{oc} [V]	*FF*	E_c [eV]	E_g [eV]
MDMO-PPV	no	3.9	0.83	0.53	1.65	1.22
'High T_g'-PPV	no	3.1	0.82	0.40	1.63	1.23
MDMO-PPV	yes	1.7	0.68	0.34	1.83	1.11
'High T_g'-PPV	yes	2.8	0.69	0.39	1.79	1.14

2.4. Influence of the Composition Ratio on E_g and V_{oc}

In previous reports it was demonstrated that V_{oc} varies with the polymer:PCBM composition ratio. In the case of MDMO-PPV it was shown that V_{oc} decreases with increasing PCBM content.[30] To varify if this effect can also be attributed to a change in E_g, FTPS was performed on four solar cells of MDMO-PPV with different weight percentages of PCBM (5, 10, 50 and 80%).

The results are summarized in Table 4 and shown in Figure 6. Again, V_{oc} and E_g follow the same trend. Upon increasing PCBM concentration, a redshift of the CT band and a proportional decrease in V_{oc} are observed.

ADVANCED FUNCTIONAL MATERIALS

Table 4. Solar cell characteristic parameters for photovoltaic BHJ devices consisting of freshly prepared MDMO-PPV:PCBM blends with a different weight fractions of PCBM.

PCBM weight fraction [%]	J_{sc} [mA.cm^{-2}]	V_{oc} [V]	FF	E_c [eV]	E_g [eV]
5	0.062	0.97	0.23	1.87	1.34
10	0.13	0.91	0.23	1.83	1.32
50	2.6	0.88	0.30	1.69	1.27
80	3.9	0.83	0.53	1.65	1.22

These results indicate that the addition of PCBM in MDMO-PPV:PCBM blends stabilizes the CT state, possibly by dipole-induced dipole interactions and/or by lowering the effective LUMO-level of PCBM due to the formation of PCBM clusters. The exact influence of both effects on the spectral position of the CT band is currently under investigation.

2.5. Relation between E_g and V_{oc}

Figure 7 summarises the overall results of the studies. It depicts the relation between E_g and V_{oc} of the polymer:PCBM devices at room temperature.

The excellent correlation found clearly indictates that the energy E_g, as defined in Equation (1), determines V_{oc}. Upon applying a linear fit, we obtain:

$$V_{oc} \approx \frac{E_g}{e} - 0.43\text{V} \quad (2)$$

The onset of 0.43 V is expected to be illumination and temperature dependent. It can mainly be attributed to voltage losses at the ITO/PEDOT:PSS and Ca/Al ohmic contacts. The band bending at these ohmic contacts reduces V_{oc} at room temperature and under 1 sun illumination by typically 0.2 V for each contact.[31]

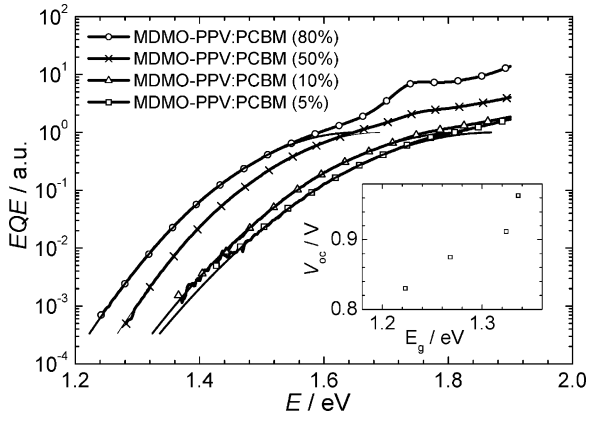

Figure 6. FTPS spectra of MDMO-PPV blended with different weight fractions of PCBM in the spectral area $1.2 < E < 2.0$ eV. The CT absorption band was fitted with a Gaussian and the effective band gap was determined as described in the text. The inset shows the open-circuit voltage V_{oc} versus the effective band gap E_g.

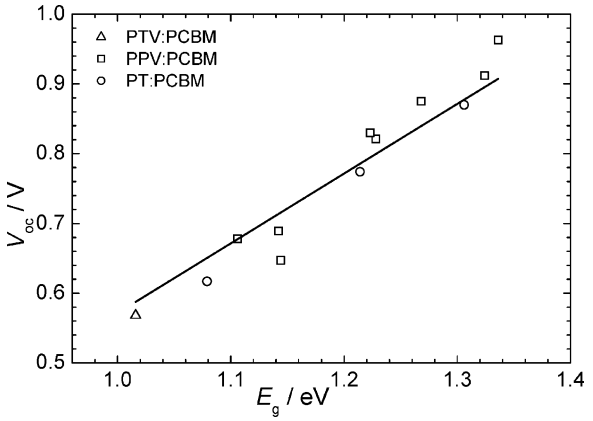

Figure 7. The effective band gap E_g versus V_{oc} of all the studied photovoltaic devices.

3. Conclusions

We have observed the formation of ground state CTCs in blends of a range of PPVs, regiorandom and regioregular P3HT and a soluble PTV derivative, all blended with PCBM. Due to its high sensitivity, FTPS enables the measurement of the photocurrent generated by the direct long wavelength absorption of the CTC, which typically has a very low absorption coefficient. The CT photocurrent band can be fitted with a Gaussian function and from the onset of the band, an effective band gap E_g for the blend can be determined. The size of E_g not only depends on the tabulated energetic position of the LUMO(A) – HOMO(D) energy differences, but also on the PCBM weight fraction and on the morphological and electronic effect of thermal annealing and aging procedures.

While the band gap of the polymer determines the spectral overlap with the solar spectrum and thus the maximum obtainable J_{sc}, we have found that there is a linear correlation between E_g as determined from the onset of the photocurrent generated by CT absorption and the V_{oc} of the solar cells. These findings go one step further than the widely accepted correlation of the open-circuit voltage with the LUMO(A) - HOMO(D) difference, as it is shown that our proposed correlation can also explain variations in V_{oc}, observed for different preparation and aging conditions of the same polymer:PCBM material system.

EQE measurement by FTPS proves to be a valuable technique because it can determine both maximum obtainable short-circuit photocurrent and maximum obtainable open-circuit voltage for a given polymer:PCBM combination in one single, fast measurement. These findings may open up new research windows that help engineering next generation solar cell organic materials.

4. Experimental

Materials: PCBM was purchased from Solenne, P3HT (ReRa and RR) from Rieke Metals and MDMO-PPV and "High T_g - PPV" [32] from Merck. Synthesis of PEO-OC9-PPV [33] and diHexyl-PTV [34] were described elsewhere.

Device Construction: Organic devices with an active layer of MDMO-PPV, PCBM and the polymer:PCBM blends were constructed using a standard procedure in N_2 atmosphere. First, a 40 nm thick poly(3,4-ethylenedioxythiophene:polystyrenesulfonate (PEDOT:PSS, Bayer) layer was spincoated from an aqueous solution onto indium tin oxide (ITO, 100 nm) coated glass. These substrates were dried for 20 min on a hotplate at 120 °C. Subsequently the active layers of the pure and blended materials were spincoated from a chlorobenzene solution on top of the PEDOT:PSS layer. Finally, 20 nm of Ca and 60 nm of Al was evaporated through a shadow mask as top electrode. All devices have an active area of 25 mm^2.

Device Measurement: All measurements were performed in N_2 atmosphere.

The IV-characteristics were measured under illumination with an Oriel solar simulator equipped with a Xenon Short Arc lamp with a power of 150W, using a home built setup with a Keithley 2004 current voltage source meter.

Thin film electrochemical properties were measured using a conventional three electrode cell with an Ag/Ag^+ reference electrode, a platinum counter electrode and an ITO coated glass substrate as working electrode. Cyclic voltamograms were recorded at 50 mV/s under N_2 atmosphere.

For the FTPS measurements, the modulated illumination beam of a Thermo Electron Nicolet 8700 FTIR with an external detector option was used. For the absolute photocurrent or *EQE* measurements via FTPS, a calibrated silicon photodetector was used as reference detector. More experimental details involving the FTPS setup are described in [35].

Received: January 11, 2008
Revised: March 13, 2008

[1] S. Günes, H. Neugebauer, N. S. Saricifti, *Chem. Rev.* **2007**, *107*, 1324.
[2] B. C. Thompson, J. M. J. Fréchet, *Angew. Chem. Int. Ed.* **2008**, *47*, 58.
[3] S. Shaheen, C. J. Brabec, N. S. Saricifti, F. Padinger, T. Fromherz, J. C. Hummelen, *Appl. Phys. Lett.* **2001**, *78*, 841.
[4] T. Munters, T. Martens, L. Goris, V. Vrindts, J. V. Manca, L. Lutsen, W. De Ceuninck, D. Vanderzande, L. De Schepper, J. Gelan, N. S. Saricifti, C. J. Brabec, *Thin Solid Films* **2002**, *403-404*, 247.
[5] O. Inganäs, M. Svensson, F. Zhang, A. Gadisa, N. K. Persson, X. Wang, M. R. Anderson, *Appl. Phys. A* **2004**, *79*, 31.
[6] A. Gadisa, W. Mammo, L. M. Andersson, S. Admassie, F. Zhang, M. R. Andersson, O. Inganäs, *Adv. Funct. Mater.* **2007**, *17*, 3836.
[7] W. L. Ma, C. Yang, X. Gong, K. Lee, A. J. Heeger, *Adv. Funct. Mater.* **2005**, *15*, 1617.
[8] J. Peet, J. Y. Kim, N. E. Coates, W. L. Ma, D. Moses, A. J. Heeger, G. C. Bazan, *Nat. Mater.* **2007**, *6*, 497.
[9] P. W. M. Blom, V. D. Mihailetchi, L. J. A. Koster, D. E. Markov, *Adv. Mater.* **2007**, *19*, 1551.
[10] A. Gadisa, M. Svensson, M. R. Andersson, O. Inganäs, *Appl. Phys. Lett.* **2004**, *84*, 1609.
[11] M. C. Scharber, D. Mühlbacher, M. Koppe, P. Denk, C. Waldauf, A. J. Heeger, C. J. Brabec, *Adv. Mater.* **2006**, *18*, 789.
[12] I.-W. Hwang, C. Soci, D. Moses, Z. Zhu, D. Waller, R. Gaudiana, C. J. Brabec, A. J. Heeger, *Adv. Mater.* **2007**, *19*, 2307.
[13] Y. Kanai, Y. C. Grossman, *Nano Lett.* **2007**, *7*, **1967**.
[14] V. D. Mihailetchi, L. J. A. Koster, P. W. M. Blom, C. Melzer, B. de Boer, J. K. J. van Duren, R. A. J. Janssen, *Adv. Funct. Mater.* **2005**, *15*, 795.
[15] L. Goris, K. Haenen, M. Nesladek, P. Wagner, D. Vanderzande, L. De Schepper, J. D'Haen, L. Lutsen, J. V. Manca, *J. Mater. Sci.* **2005**, *40*, 1413.
[16] L. Goris, A. Poruba, L. Hod'akova, M. Vanecek, K. Haenen, M. Nesladek, P. Wagner, D. Vanderzande, L. De Schepper, J. V. Manca, *Appl. Phys. Lett.* **2006**, *88*, 052113.
[17] R. Foster, in: *Organic Charge-Transfer Complexes*, Academic Press, New York **1969**.
[18] D. V. Konarev, R. N. Lyubovskaya, N. V. Drichko, V. N. Semkin, A. Graja, *Russ. Chem. Bull.* **1999**, *48*, 3.
[19] P. Panda, D. Veldman, J. Sweelssen, J. J. A. M. Bastiaansen, B. M. W. Langeveld-Voss, S. C. J. Meskers, *J. Phys. Chem.* **2007**, *111*, 5076.
[20] M. A. Loi, S. Toffanin, M. Muccini, M. Forster, U. Scherf, M. Scharber, *Adv. Funct. Mater.* **2007**, *17*, 2111.
[21] J. J. Benson-Smith, L. Goris, K. Vandewal, K. Haenen, J. V. Manca, D. Vanderzande, D. D. C. Bradley, J. Nelson, *Adv. Funct. Mater.* **2007**, *17*, 451.
[22] M. Vaněček, A. Poruba, *Appl. Phys. Lett.* **2002**, *80*, 719.
[23] H. Ohkita, S. Cook, Y. Astuti, W. Duffy, S. Tierney, W. Zhang, M. Heeney, I. McCulloch, J. Nelson, D. D. C. Bradley, J. R. Durrant, *J. Am. Chem. Soc.* **2008**, *130*, 3030.
[24] R. A. Marcus, *J.Phys.Chem.* **1989**, *93*, 3078.
[25] R. A. Marcus, *J.Phys.Chem.* **1990**, *94*, 4963.
[26] M. Reyes-Reyes, K. Kim, D. L. Carroll, *Appl. Phys. Lett.* **2005**, *87*, 083506.
[27] P. Vanlaeke, A. Swinnen, I. Haeldermans, G. Vanhoyland, T. Aernouts, D. Cheyns, C. Deibel, J. D'Haen, P. Heremans, J. Poortmans, J. V. Manca, *Sol. Energy Mater. Sol. Cells* **2006**, *90*, 2150.
[28] S. Bertho, I. Haeldermans, A. Swinnen, W. Moons, T. Martens, L. Lutsen, D. Vanderzande, J. V. Manca, A. Senes, A. Bonfiglio, *Sol. Energy Mater. Sol. Cells* **2007**, *91*, 385.
[29] T. Q. Nguyen, I. B. Martini, J. Liu, B. J. Schwartz, *J. Phys. Chem. B* **2000**, *104*, 237.
[30] J. K. J. Van Duren, X. Yang, J. Loos, C. W. T. Bulle-Lieuwma, A. B. Sieval, J. C. Hummelen, R. A. J. Jannsen, *Adv. Funct. Mater.* **2004**, *14*, 425.
[31] V. D. Mihailetchi, P. W. M. Blom, J. C. Hummelen, M. T. Rispens, *J. Appl. Phys.* **2003**, *94*, 6849.
[32] H. Becker, H. Spreitzer, W. Kreuder, E. Kluge, H. Schenk, I. Parker, Y. Cao, *Adv. Mater.* **2000**, *12*, 42.
[33] M. Breselge, I. Van Severen, L. Lutsen, P. Adriaensens, J. Manca, D. Vanderzande, T. Cleij, *Thin Solid Films* **2006**, *511-512*, 328.
[34] F. Banishoeib, S. Fourier, T. J. Cleij, L. Lutsen, D. Vanderzande, *Eur. Phys. J. Appl. Phys.* **2007**, *37*, 237.
[35] K. Vandewal, L. Goris, I. Haeldermans, M. Nesládek, P. Wagner, J. V. Manca, *Thin Solid Films* **2007**, in press